INSTITUTE OF PHYSICS PUBLISHING PHYSICS IN MEDICINE AND BIOLOGY

Phys. Med. Biol. **49** (2004) 1147–1163 PII: S0031-9155(04)74367-5

Sagittal laser optical tomography for imaging of rheumatoid finger joints

Andreas H Hielscher[1], Alexander D Klose[1], Alexander K Scheel[2], Bryte Moa-Anderson[1], Marina Backhaus[3], Uwe Netz[4] and Jürgen Beuthan[4]

[1] Departments of Biomedical Engineering and Radiology, Columbia University, New York, NY 10027, USA
[2] Department of Nephrology and Rheumatology, Georg-August University, Göttingen, Germany
[3] Department of Rheumatology and Clinical Immunology, Charité University Hospital, Berlin, Germany
[4] Institute for Medical Physics and Laser Medicine, Free University of Berlin, Berlin, Germany

E-mail: ahh2004@columbia.edu

Received 3 October 2003
Published 18 March 2004
Online at stacks.iop.org/PMB/49/1147 (DOI: 10.1088/0031-9155/49/7/005)

Abstract

We present a novel optical tomographic imaging system that was designed to determine two-dimensional spatial distribution of optical properties in a sagittal plane through finger joints. The system incorporates a single laser diode and a single silicon photodetector into a scanning device that records spatially resolved light intensities as they are transmitted through a finger. These data are input to a model-based iterative image reconstruction (MOBIIR) scheme, which uses the equation of radiative transfer (ERT) as a forward model for light propagation through tissue. We have used this system to obtain tomographic images of six proximal interphalangeal finger joints from two patients with rheumatoid arthritis. The optical images were compared to clinical symptoms and ultrasound images.

1. Introduction

Over the last ten years diffuse optical tomography (DOT) has made big strides towards becoming a novel viable biomedical imaging modality (Tromberg and Yodh 2000, 2002, Chance *et al* 1999, 2001). Currently this technology is mainly applied towards brain and breast imaging (Obrig and Villringer 2003, Gratton *et al* 2003, Franceschini *et al* 2003, Siegel *et al* 2003, Wang *et al* 2003, Hebden 2003, Benaron *et al* 2000, Pifferi *et al* 2003, Culver *et al* 2003, Li *et al* 2003a, 2003b, Pera *et al* 2003, Grosenick *et al* 2003, Xu *et al* 2003). Another promising application is imaging of joint diseases (Henniger *et al* 2003, Beuthan *et al* 2001, 2002, Xu *et al* 2001, 2002b, Klose *et al* 1997, 1998, Prapavat *et al* 1997). The small

dimensions of, for example, finger joints results in much higher transmitted light intensities as compared to breast or brain imaging, and consequently result in better signal to noise ratios. This should lead in principle to much better image quality and higher spatial resolution as compared to optical tomographic breast or brain imaging. However, research in this area has been limited to numerical studies and the analysis of transmitted data without tomographic reconstruction. Scheel *et al* (2002) and Schwaighofer *et al* (2003) recently demonstrated that the information contained in optical transmission data can be used to monitor changes in the disease state of inflamed joints of patients with rheumatoid arthritis. They obtained a baseline measurement during a first visit and then compared the transmission measurements obtained at subsequent visits to the results of the first visit. In this way they were able to detect improvements or deterioration in the disease status. But Scheel and Schwaighofer did not attempt tomographic reconstructions and they were unable to optically diagnose the degree of joint inflammation directly. A promising system for tomographic images of joints and bones has so far only been reported by Xu *et al* (2001, 2002b). However, this group has not employed their system for the detection of any specific joint disease and used a coronal imaging plane.

The goal of this work was to develop a sagittal laser optical tomographic (SLOT) imaging system for the diagnosis and monitoring of inflammatory processes in proximal interphalangeal (PIP) joints of patients with rheumatoid arthritis, without the need for a baseline measurement. Rheumatoid arthritis (RA) is a chronic, progressive, inflammatory disease, which primarily attacks peripheral joints and surrounding tendons and ligament (Norris 1998). Different disease stages can be distinguished, during which the tissue change is gradually from mild inflammation of the synovial membrane (synovitis) to fibrous tissue calcifies that lead to immobility of the joint (Steinbrocker *et al* 1949, Harris 1990). The synovial tissue becomes infiltrated with inflammatory cells and activated, invasive fibroblast-like cells, which may invade bone and cartilage. RA affects approximately 2.1 million people in the United States (Lubeck 1995, Harris 1990, NCHS 1984). Mortality rates for people with RA are double that of the general population, and medical costs and indirect expenses due to lost wages for RA are estimated at over US$ 3 billion annually. Less than 50% of working age adults with RA are still employed ten years after disease onset.

The diagnosis of RA is currently based on the patient's history, physical examination, laboratory studies and radiographs (Arnett *et al* 1988, Semble 1995). During the physical examination, physicians take into account location, degree and frequency of soft tissue swelling, patients complains of morning stiffness and existence of rheumatoid nodules. Laboratory studies usually involve the determination of erythrocyte sedimentation rate (ESR) and c-reactive protein (CRP). Both parameters are obtained from blood tests. ESR and CRP are elevated in most RA patients with disease activity (Wolfe *et al* 2001), however these values can also be raised in patients with other infectious disease. Synovial fluid analysis typically reveals increased volume and turbidity, but decreased viscosity and complement (C3 and C4) levels. The white blood cell count in the synovial fluid commonly exceeds $10\,000/\mu$l However, an analysis of the synovial fluid is rarely carried out in finger joints, because of the limited amount of fluid in these joints.

Of all imaging modalities, radiography has the best-established role in the assessment of the severity of RA (Brown and Deluca 1995). Radiography can document the bone damage that results from RA and visualizes the narrowing of cartilage spaces. However, it has long been recognized that radiography is insensitive to bone damage at its earlier stages and is incapable of capturing the primary feature of rheumatoid disease, the inflammation of the synovial membrane, commonly referred to as synovitis (Ostergaard and Szkudlarek 2003). MRI can be employed to assess soft tissue problems (Winalski *et al* 1996, Ostergaard *et al* 1997, 2001, Graham *et al* 1997, Boutry *et al* 2003, Backhaus *et al* 2002). But, for the detection

of inflammatory soft tissue changes, gadolinium has to be used as contrast agent, and therefore this technique becomes invasive. Overall the high costs of MRI, the need for contrast agents and the cumbersome use (long data-acquisition times during which patient needs to be immobilized) have prevented MRI from becoming a routinely used RA imaging modality. Several groups are currently evaluating ultrasound as a tool for the diagnosis of arthritic changes (Schmidt *et al* 2003, Backhaus *et al* 1999, Fiocco *et al* 1996, Lund *et al* 1995, Szkudlarek *et al* 2003b, Tan *et al* 2003, Ostergaard and Szkudlarek 2003). It has been shown that joint effusion can be detected as increased fluid in between the bone and the capsula, which often appears in combination with hypertrophy of the synovial membrane. Both phenomena are thought to be related to synovitis. The downside of joint ultrasonography is that the examinations are typically time consuming, and image acquisition and correct reading of the images requires considerable operator training and experience.

Optical techniques promise to provide a new approach to early detection and monitoring of joint inflammation in patients with RA. For example, the normally clear yellowish synovial fluid turns into a turbid greyish substance early in the inflammatory process. Furthermore, changes in the vasculature and haemodynamics surrounding the joint have been observed. So far, however, groups have not been able to make a diagnosis solely based on optical methods, without a reference measurement. The goal of this work is to go beyond previous numerical, phantom and clinical studies and to demonstrate the feasibility of optical tomographic techniques to distinguish between joints with and without clinical symptoms of joint inflammation. If clinical utility can be proven optical tomographic imaging would present a low-cost, easy-to-operate adjunct or even an alternative to existing techniques.

Besides presenting a detailed description of a newly developed optical measurement system and the model-based iterative image reconstruction scheme, we will discuss in detail two cases of RA patients clinically diagnosed with synovitis in several PIP joints. The optical tomographic images are compared to clinical findings, laboratory parameters and ultrasound measurements.

2. Methods

2.1. Instrumentation

To determine the optical properties in a sagittal section through the joint, we have developed a device that allows for measuring with high accuracy light transmission profiles. A scheme of the device is shown in figure 1. The experimental set-up consists of a $30 \times 30 \times 30$ cm box for placing and positioning the hand and finger in a warm water bath. The instrument incorporates a diode laser featuring a wavelength of $\lambda = 650$ nm (S6515MG, Roithner Lasertechnik, Wien, Austria, driver: iC-JW, iC-Haus GmbH, Bodenheim, Germany, mean optical power: 3 mW, exit pupil: 1 mm diameter, aperture angle: 2.3°), a silicon (Si) photodetector (Si pin photodiode TSL253, TOAS Inc., Plano, Texas, entrance pupil: 2 mm diameter, aperture angle 25°) and two stepping motor-driven translation stages (OWIS, Staufen, Germany) that are used to move the laser diode and photodetector to the desired measurement positions. During a measurement, light from the diode laser is focused on a spot of approximately 0.3 mm in diameter on the back of the finger. The photodiode, which is immersed in the water and in direct contact with the palmar side of the finger, is then scanned over a distance of up to 3 cm and the transmitted intensities are detected along a sagittal plane. After the detector scan is finished, the diode laser is moved by a distance of Δx, and the photodiode performs another scan, etc. In this way several transmission profiles are obtained (figure 2). A lock-in technique is used to suppress any broadband noise and any interference of ambient light when

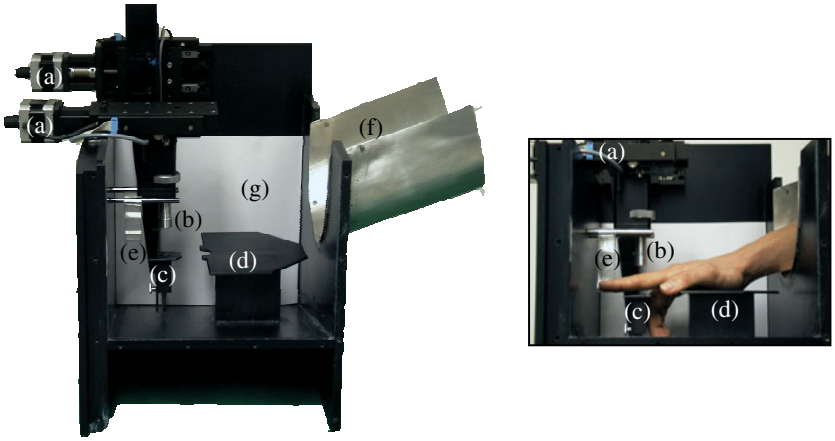

Figure 1. Sagittal laser optical tomographic (SLOT) imaging system: (a) stepping motors, (b) diode laser ($\lambda = 650$ nm), (c) photodetector, (d) hand rest, (e) finger holder, (f) arm rest and (g) water tank.

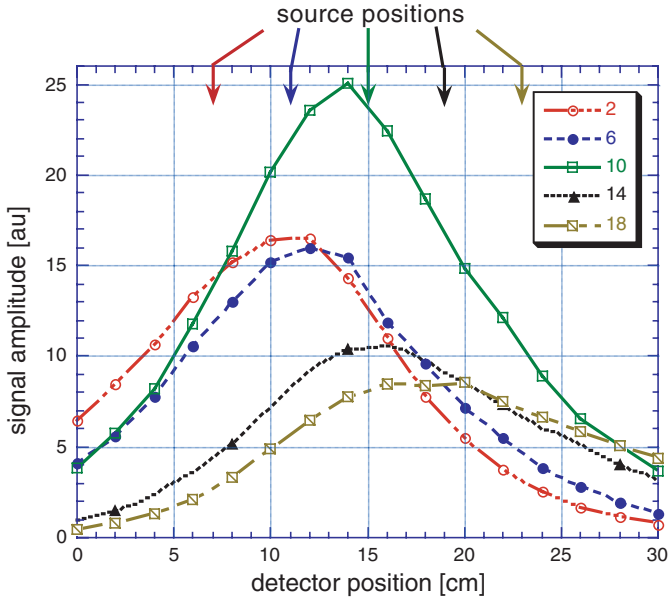

Figure 2. Intensity transmission profiles obtained by focusing a diode laser ($\lambda = 650$ nm) onto five different positions on the dorsal side of a finger and measuring the transmitted intensities at multiple positions on the palmar side. Source position 2 is closest to the finger tip, while source position 18 is the farthest from the finger tip. Source position 10 is located directly above the PIP joint.

the signal of the photodetector is detected. For this purpose the diode laser is operated with a sinusoidal current modulation at 3.4 kHz. Using a lock-in amplifier card (LIA-150, Becker & Hickl, Berlin, Germany), the signal is directly read into a computer and processed by means of a special-purpose software. The typical time for a full data acquisition is about 4 min, assuming that for each of ten different source positions on the back of the finger, transmitted

light intensities are measured at 16 different detector positions. Since no optical fibres are used and the same source and detector are employed for each measurement, the recorded profiles can be directly compared to each other without additional calibrations for fibre incoupling losses, different source strengths or detector sensitivities.

2.2. Image reconstruction algorithm

The measured data are input to a model-based iterative image reconstruction (MOBIIR) scheme (Hielscher *et al* 1999), which uses the equation of radiative transfer,

$$\Omega\nabla\Psi\,(r,\Omega) + (\mu_a(r) + \mu_s(r))\,\Psi\,(r,\Omega) = S\,(r,\Omega) + \mu_s \int_{4\pi} p(\Omega,\Omega')\Psi(r,\Omega')\,\mathrm{d}\Omega'$$

as a forward model (Klose and Hielscher 1999, 2002, Klose *et al* 2002). The quantity $\Psi(r, \Omega)$ is the radiance at the spatial position r, which is directed into a solid unite angle Ω, with units of W cm^{-2} sr^{-1}. Other quantities are the source term that describes the strength, position and direction of the incident light, the scattering coefficients μ_s, the absorption coefficient μ_a, both given in units of cm^{-1} and the scattering phase function $p\,(\Omega; \Omega')$.

Given an initial guess of the spatial distribution of the optical parameters $\mu(r) = (\mu_\mathrm{a}\,(r), \mu_\mathrm{s}(r))$ as well as the source term S, we solve this equation by using a discrete-ordinate, finite-difference, upwind scheme. The solution provides $\Psi(r, \Omega)$ for all r and Ω, including the energy radiance Ψ_d on the boundary, from which we can derive numerically predicted measurement data by integrating over the numerical aperture Γ_{NA} of the detector,

$$\Psi_{s,d}(\mu) = \Psi(r_d) = \int_{\Gamma_{NA}} \Psi(r,\Omega).$$

A given set of measurements M on the boundary is then compared with the set of the predicted $\Psi_{s,d}(\mu)$ by defining an objective function Θ. In this work, we use the least square error norm between measured and predicted data given by

$$\Theta = \sum_s \sum_d (M_{s,d} - \Psi_{s,d}(\mu))^2 \big/ M_{s,d}^2.$$

To determine the spatial distribution of optical properties that leads to the best agreement between predicted and measured data, the objective function Θ is minimized by iteratively updating the distribution of optical properties according to

$$\mu_{k+1} = \mu_k + \alpha_k \cdot u_k$$

where μ_k is a vector containing a set of optical properties from which the new set μ_{k+1} is obtained. The vector u_k is a search direction in N-dimensional space, given a problem with N unknowns. The parameter α_k is the step length in the direction u_k. To obtain u_k and α_k, we employ the so-called limited-memory Broyden–Fletcher–Goldfarb–Shanno (BFGS) minimization scheme (Klose and Hielscher 2003), in which the derivative $\mathrm{d}\,\Theta/\mathrm{d}\mu$ of the objective function with respect to the optical properties is used to determine the search direction. This gradient is computed by an adjoint differentiation technique (Klose and Hielscher 2002). The iteration process is finished when the minimum of the objective function is reached within a specified error. At this point the predicted detector readings are identical to the measured detector readings within a given tolerance. The optical parameters, μ, are mapped into a two- or three-dimensional images. In this work we employ a two-dimensional transport model. For more details concerning this technique we refer to references Hielscher *et al* (1999), Klose and Hielscher (1999, 2002, 2003) and Klose *et al* (2002).

2.3. Clinical and laboratory assessment

Two patients were recruited from the rheumatologic outpatient clinic of the Charité University Hospital, Department of Medicine, Rheumatology and Clinical Immunology. All PIP joints were examined by a trained physician for clinically and ultrasonographic signs of synovitis. Additionally, several laboratory parameters were assessed to evaluate the overall disease activity. The study was approved by the local ethical committee, and the patients gave informed consent prior to investigation.

Clinical examination of each PIP joint was performed by bi-manual palpation to assess the degree of swelling, tenderness and warmth. The joints were classified according to clinical synovitis score (CSS) ranging from 0 to 3. A joint received a CSS = 0 (not involved) when there were no signs of swelling, tenderness or warmth. A CSS = 3 (significantly involved) indicated a joint that was considerably swollen, very tender and very warm. Joints that displayed some swelling, tenderness or warmth were classified as CSS = 1 (minimally involved), or CSS = 2 (moderately involved), depending on the severity of the symptoms.

To assess the overall state of the disease, ESR and CRP tests were performed. Higher sedimentation rates indicate the presence of inflammation and occur in inflammatory disease, such as RA. The CRP is a protein build in liver tissue and also considered a parameter of inflammation as part of activating the immune system. Although not specific, both parameters show a good correlation to rheumatoid arthritis disease activity (Wolfe *et al* 2001).

Finally, an overall disease activity score (DAS) was assessed. The DAS28 is a combined index that has been developed to measure the disease activity in patients with RA (Fuchs *et al* 1989, Prevoo *et al* 1995). It includes a classification of 28 joints according to the degree of swelling and tenderness, ESR and a patient's self-assessment according to the visual analogue scale. The DAS28 results in a number between 0 and 10, indicating how active the RA is at this moment. Using the DAS28, several thresholds have been developed for high disease activity, low disease activity or disease inactivity. Disease activity is defined as inactive when DAS28 $\leqslant$ 3.2, moderately active if 3.2 $<$ DAS28 $<$ 5.1 and highly active if DAS28 $>$ 5.1.

2.4. Ultrasound imaging

Ultrasound (US) images were obtained for each joint by using a multi-frequency (5 to 10 MHz) hockey stick transducer (ATL, HDI 3500, Bothell, WA, USA) that was placed on the palmar side of the joint. We found that, most likely due to the lack of sufficient muscular tissue, measurements from the dorsal side often show imaging artefacts and are less reliable. There are two features in US images relevant for the assessment of joint involvement in RA. First joint effusion is visible as a black anechoic structure between the capsule and the bone (see, for example, area marked as (1) in figure 3(d)). Second a thickening of the synovial membrane (hypertrophy) can lead to hyperechoic structures within the region affected by effusion (see, for example, area marked as (2) in figure 3(e)). The degree of joint effusion and hypertrophy were evaluated and classified on a four-grade semiquantitative ultrasound examination score (USS) according to Szkudlarek *et al* (2003a). When no anechoic structure was visible the trained physician assigned USS = 0 (no effusion/hypertrophy). The larger the anechoic structure or extent of synovial hypertrophy as observed in the US images the higher USS (USS = 1 (minimal effusion/hypertrophy); USS = 2 (moderate effusion/hypertrophy) and USS = 3 (extensive effusion/hypertrophy). Examples of for scores of 0, 2 and 3 can be seen in figure 3. The bottom row (figures 3(c) and (f)) shows two examples for USS = 0. The dominating feature in these two images is the white line that undulates from the left to the

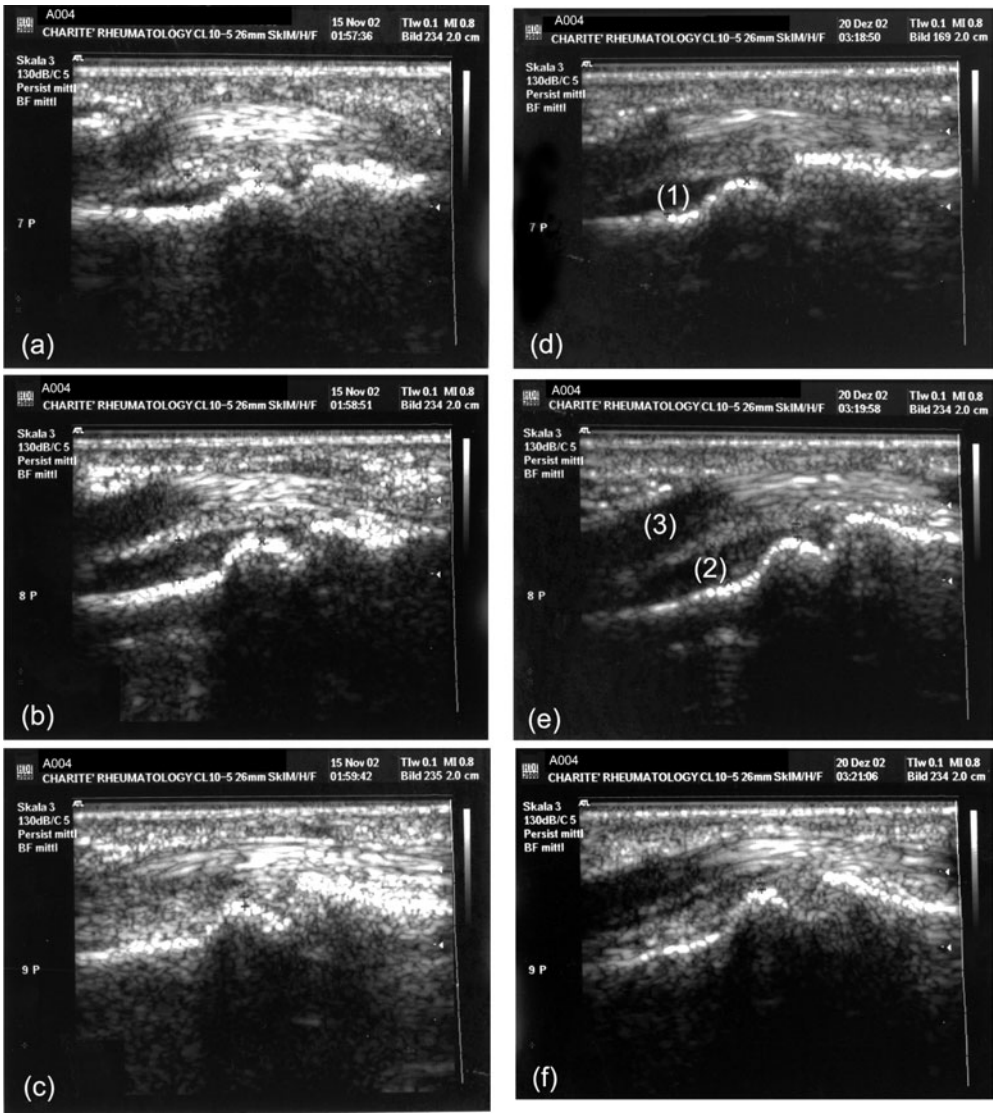

Figure 3. Ultrasound images of the index finger (top row), middle finger (middle row) and ring finger (bottom row) of the right hand of patient 1. Each of the images shows a cross-sectional area of $\sim$15 mm $\times$ 10 mm. The images in the left row were obtained during the first visit, while the images in the right row were obtained six weeks later during the second visit. Note that the images are obtained palmar, therefore the inside of the hand is shown towards the top of each image.

right. This line is indicative of an echogenic interface, here the surface of the bones is adjacent to the joint. Note that directly above the white line no anechogenic mass is visible. The black area marked as (3) in figure 3(e) is part of the tendon and does not indicate effusion. This anechoic area is caused by the particular angle of the transducer to the tendon, which has an anisotropic tissue structure. Effusion is clearly visible in images in the middle row (figures 3(b) and (e)) as a dark area just above the bone. This joint is an example for the case of extensive

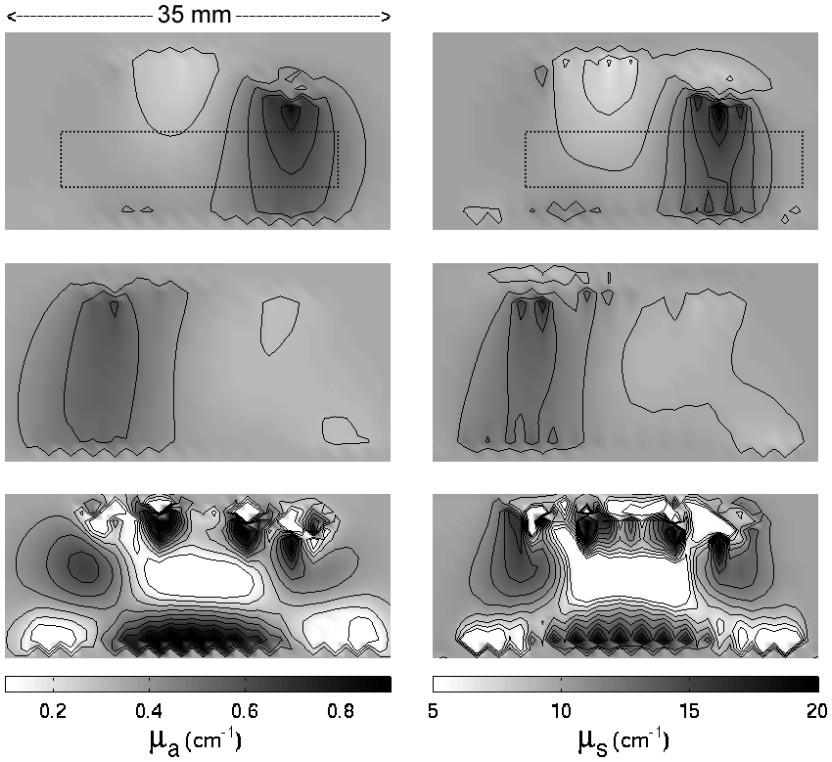

Figure 4. Absorption and scattering images in a sagittal plane through the index finger (top row), middle finger (middle row) and ring finger (bottom row) of the right hand of patient 1. The images were obtained during the first visit. (Compare to US images in figures 3(a), (b) and (c).)

effusion (USS = 3). The effusion area is somewhat smaller in figures 3(a) and (d) (top row), which show a joint that the physician scored as USS = 2.

3. Results

3.1. Case 1

We first discuss the case of a 54 year old female, who was first diagnosed with RA in 1997. Three PIP joints of the right hand were examined at two different days, approximately six weeks apart in November and December 2002. The DAS28 scores were 6.67 and 5.66, respectively, while ESR equaled 99 and 23; CRP was found to be 3.5 and 2.8, respectively. At both visits, the joints were assessed by the physician as CSS = 1 (index finger) CSS = 1 (middle finger) and CSS = 0 (ring finger), while the ultrasound examination resulted in USS = 2 (index finger), USS = 3 (middle finger) and USS = 0 (ring finger), respectively. The ultrasound images obtained during the first and second visits are shown figure 3.

The corresponding optical reconstructions of the absorption and scattering coefficient obtained during the first visit are shown in figure 4. The initial guess for this reconstruction was $\mu_s = 10$ cm^{-1} and $\mu_a = 0.3$ cm^{-1} and $g = 0$. The reconstruction took approximately 80 min on a LINUX workstation with a 2.2 GHz Xeon processor. One can see that the two joints with CSS = 1 and USS > 1 (index and middle fingers) are clearly distinguishable from

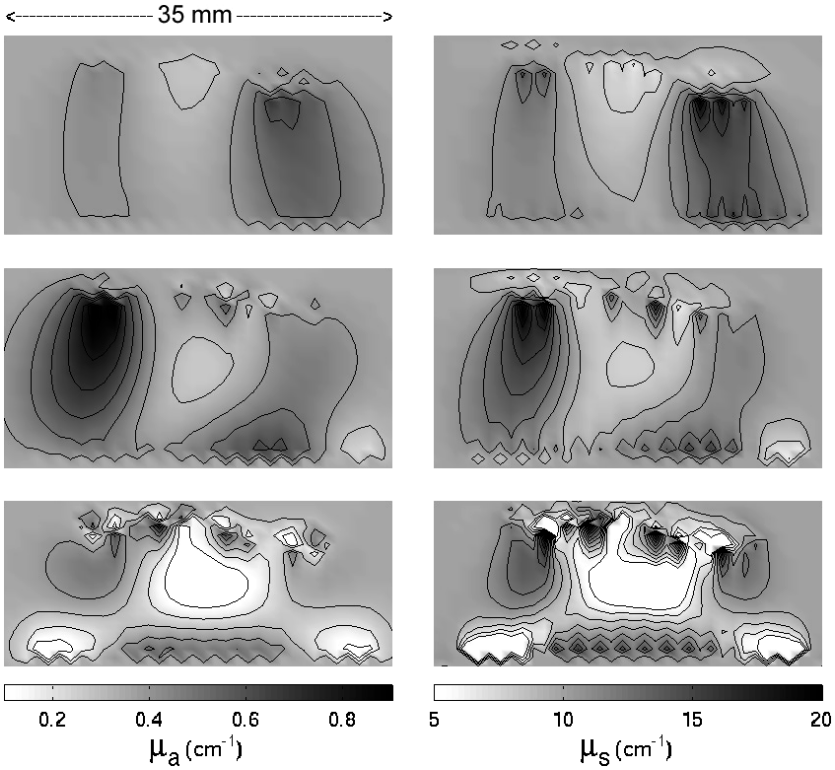

Figure 5. Absorption and scattering images in a sagittal plane through the index finger (top row), middle finger (middle row) and ring finger (bottom row) of the right hand of patient 1. The images were obtained during the second visit. (Compare to US images in figures 3(d), (e) and (f).)

the joint free of clinical and ultrasonographic symptoms of synovitis (ring finger with CSS = USS = 0). The unaffected joint shows a clear drop in optical properties in the centre of the image. The joints with clinical and ultrasonic signs of synovitis show little variation in optical properties. Besides the overall visual impression, we determined for each joint the minimum and maximum scattering coefficients in an area surrounding the joint cavity (dotted lines in figures 4(a) and (b)). The joints with symptoms showed minimal μ_s—values between 8.54 cm^{-1} and 9.06 cm^{-1}, while the unaffected joints produced a minimal scattering coefficient of $\mu_s = 0.51$ cm^{-1}. The minimal absorption coefficients of the affected joints are close to the initial guess ($\mu_a = 0.30$ cm^{-1}), while in the joint with inflammation shows $\mu_a = 0.03$ cm^{-1}. In the follow-up examination approximately six weeks later, the clinical and US scores did not change, and accordingly the optical images obtained during the second visit (see figure 5) were similar to the images generated during the first visit. The results of the clinical, ultrasonographic and optical examinations are summarized in tables 1 and 2.

3.2. Case 2

A 43 old female, who was first diagnosed with RA in 1995, was examined twice with 90 days between examinations. In the first examination all PIP joints of the left hand showed strong signs of synovitis. The CSS equaled 2, 2 and 1 for PIP joints of the index, middle and ring

Table 1. Summary of clinical, ultrasound and optical examinations during first visit of patient in case 1.

	CSS	USS	Min(μ_s) (cm^{-1})	Max(μ_s) (cm^{-1})	Min(μ_s)/ Max(μ_s)	Min(μ_a) (cm^{-1})	Max(μ_a) (cm^{-1})	Min(μ_a)/ Max(μ_a)	DAS28	ESR	CRP
Index finger	1	2	8.54	16.35	0.52	0.30	0.69	0.43			
Middle finger	1	3	9.06	13.11	0.69	0.30	0.56	0.54	6.67	99	3.5
Ring finger	0	0	0.51	15.09	0.03	0.03	0.65	0.05			

Table 2. Summary of clinical, ultrasound and optical examinations during second visit of patient in case 1.

	CSS	USS	Min(μ_s) (cm^{-1})	Max(μ_s) (cm^{-1})	Min(μ_s)/ Max(μ_s)	Min(μ_a) (cm^{-1})	Max(μ_a) (cm^{-1})	Min(μ_a)/ Max(μ_a)	DAS28	ESR	CRP
Index finger	1	2	8.49	15.33	0.55	0.32	0.59	0.54			
Middle finger	1	3	7.70	15.08	0.51	0.26	0.76	0.34	5.66	23	2.8
Ring finger	0	0	0.45	13.56	0.03	0.02	0.48	0.04			

Table 3. Summary of clinical, ultrasound and optical examinations during first visit of patient in case 2.

	CSS	USS	Min(μ_s) (cm^{-1})	Max(μ_s) (cm^{-1})	Min(μ_s)/ Max(μ_s)	Min(μ_a) (cm^{-1})	Max(μ_a) (cm^{-1})	Min(μ_a)/ Max(μ_a)	DAS28	ESR	CRP
Index finger	2	3	9.87	18.98	0.52	0.36	0.78	0.46			
Middle finger	2	3	9.86	21.91	0.45	0.37	0.89	0.41	6.91	22	2.2
Ring finger	1	2	9.64	29.18	0.33	0.38	1.14	0.32			

Table 4. Summary of clinical, ultrasound and optical examinations during second visit of patient in case 2.

	CSS	USS	Min(μ_s) (cm^{-1})	Max(μ_s) (cm^{-1})	Min(μ_s)/ Max(μ_s)	Min(μ_a) (cm^{-1})	Max(μ_a) (cm^{-1})	Min(μ_a)/ Max(μ_a)	DAS28	ESR	CRP
Index finger	0	3	6.66	15.31	0.43	0.18	0.64	0.28			
Middle finger	1	3	7.47	16.71	0.45	0.19	0.79	0.24	4.43	14	0.67
Ring finger	0	1	6.31	16.72	0.38	0.22	0.74	0.30			

fingers, respectively, while the ultrasound images yielded USS = 3, 3, 2 for the same three joints (see figures 6(a), (b) and (c)). Other disease-related parameters were determined as DAS = 6.91, ESR = 22 and CRP = 2.2. The optical tomographic images obtained during the first visit are shown in figure 7. The images of all three joints show a high scattering and absorption coefficients in the area of the joint cavity.

When the patient returned after three months her overall state had considerably improved (DAS = 4.43, ESR = 14 and CRP = 0.67). Clinical examination led to improved scores of CSS = 0, 1 and 0, for the index, middle and ring fingers, respectively. The ultrasound images (figures 6(d), (e) and (f)) also indicated an improvement for all fingers (USS = 2, 2 and 1 for index, middle and ring fingers, respectively). The optical tomographic images shown in figure 8 seem to confirm the clinical and ultrasound findings as the scattering coefficients have dropped considerably, and are now lower in the area of the joint cavity than of the bone for both fingers. For example, the minimum μ_s values dropped from 9.86 cm^{-1} to 7.47 cm^{-1} in middle finger, and from 9.64 cm^{-1} to 6.31 cm^{-1} in the ring finger (see tables 3, 4). At the same time the minimum μ_a values dropped from 0.37 cm^{-1} to 0.19 cm^{-1} and from 0.38 cm^{-1}

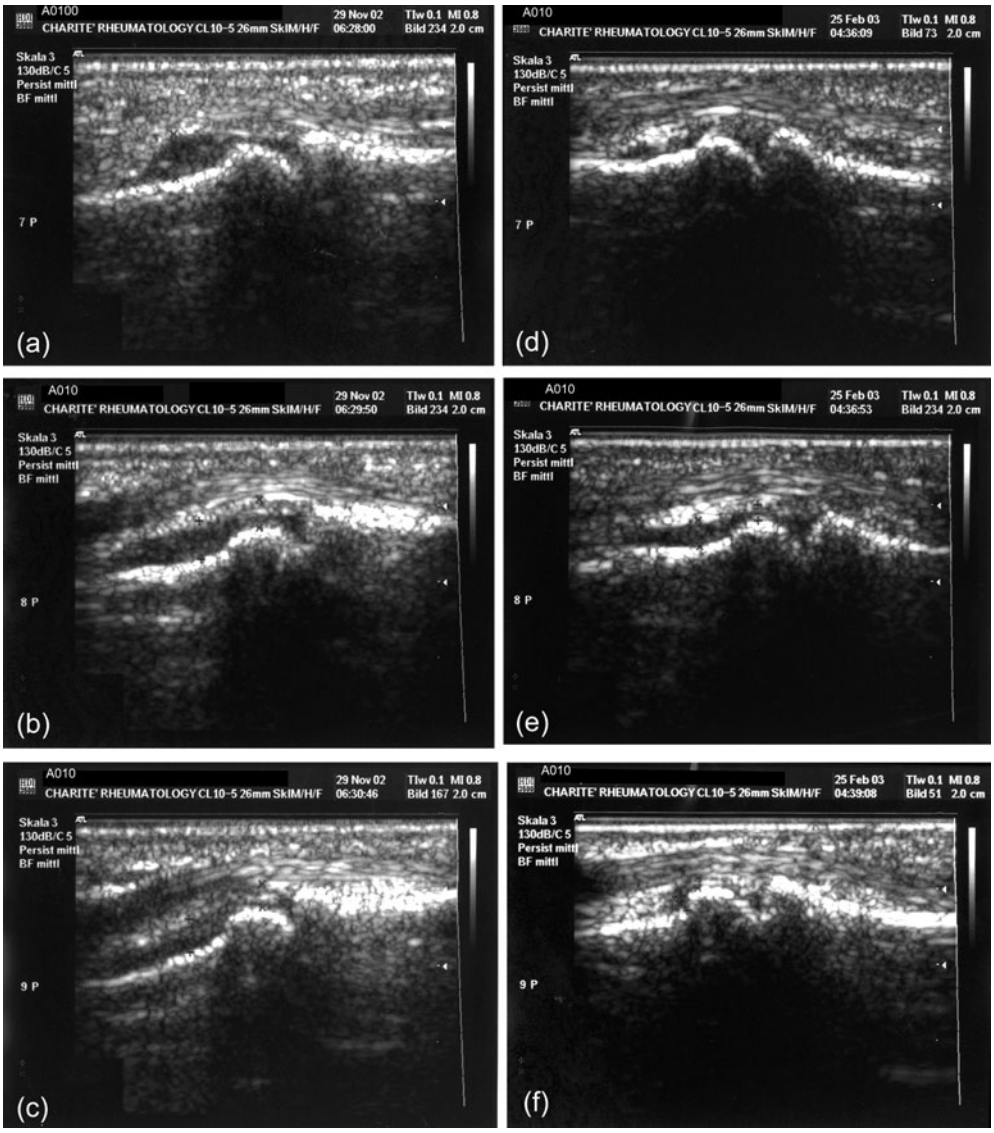

Figure 6. Ultrasound images of the index finger (top row), middle finger (middle row) and ring finger (bottom row) of the right hand of patient 2. Each of the images shows a cross-sectional area of $\sim$15 mm $\times$ 10 mm. The images in the left row were obtained during the first visit, while the images in the right row were obtained 3 months later during the second visit. Note that the images are obtained palmar, therefore the inside of the hand is shown towards the top of each image.

to 0.22 $cm^{-1.}$ The maximal μ_s values also dropped from 21.90 cm^{-1} to 16.71 cm^{-1} in the middle finger and from 29.18 cm^{-1} to 16.72 cm^{-1} in the ring finger.

4. Discussion

In general, we observe a good agreement between optical tomographic images and clinical ultrasonic findings. In the first patient, the finger joints with symptoms of synovitis as

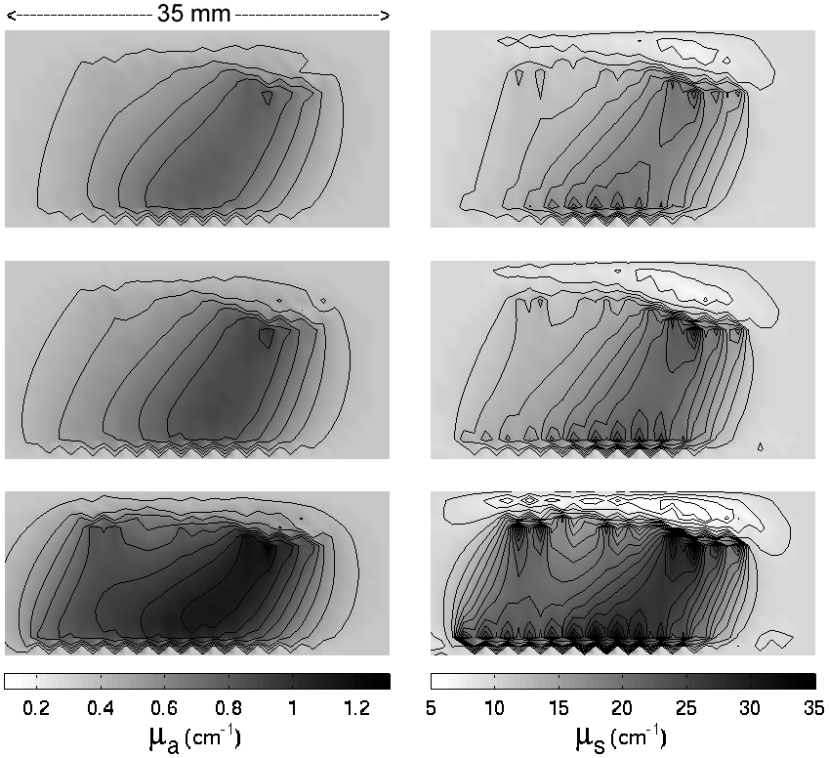

Figure 7. Absorption and scattering images in a sagittal plane through the index finger (top row), middle finger (middle row) and ring finger (bottom row) of the right hand of patient 2. The images were obtained during the first visit. (Compare to US images in figures 6(a), (b) and (c).)

identified by US imaging and clinical examinations were also identified as symptomatic by optical techniques. This case seems to affirm the hypothesis that in inflamed joints the optical properties of the synovial fluid become similar to the optical properties of the tissues surrounding the joint cavity. If a joint is free of inflammation we observe a strong drop in scattering as well as absorption in the centre of the joint. If a joint has clinical signs of inflammation this drop is almost absent and the optical properties in and near the joint cavity are similar to the optical properties of the bone. Furthermore, it is encouraging that during the follow-up visit, which showed no changes in ultrasonographic and clinical findings, the optical results of the first visit were reproduced. When changes in the disease status were clinically diagnosed, as in the second patient, optical tomographic measurements supported the findings as well.

It should be noted that clinical and ultrasound findings do not always agree. For example, in the second visit of the second patient, the physician assessed two of the three joints as not involved (CSS $= 0$ for PIP joints of index and ring fingers) and one as moderately involved (CSS $= 1$ for middle finger). At the same time the US images still show some effusion and synovial hypertrophy, which resulted in USS equal to 2, 2 and 1 for the index, middle and ring fingers, respectively. The optical images (figure 7) obtained during the second visit show some variation in the scattering and absorption coefficient but not as much as in the unaffected PIP joint of patient number 1. Therefore, the optical images seem to support the ultrasound score and not the clinical score. As already mentioned, ultrasound is sensitive to fluid built-up

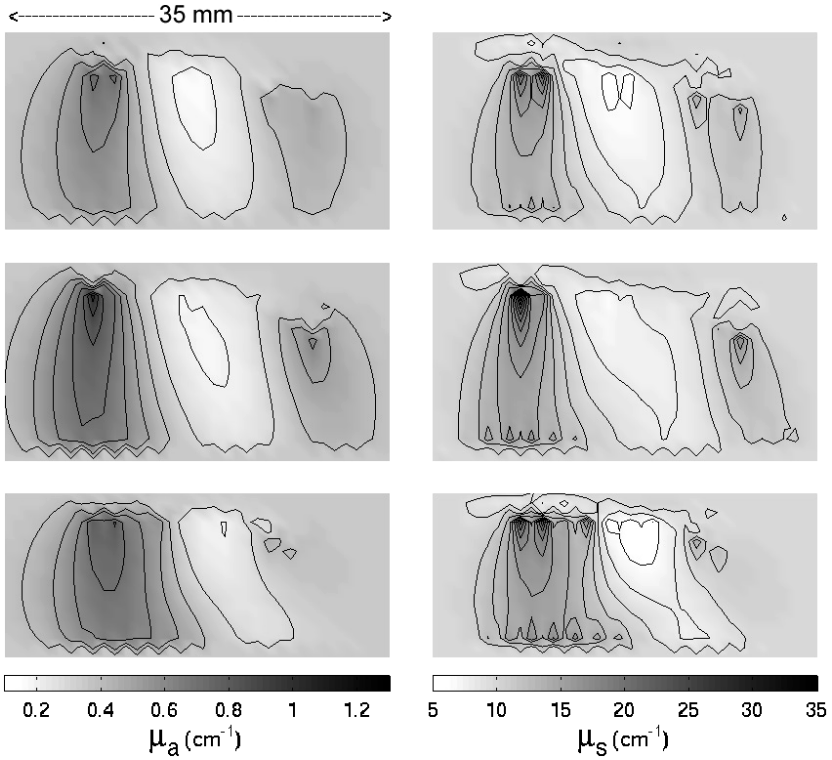

Figure 8. Absorption and scattering images in a sagittal plane through the index finger (top row), middle finger (middle row) and ring finger (bottom row) of the right hand of patient 2. The images were obtained during the second visit. (Compare to US images in figures 6(d), (e) and (f).)

(effusion) in between the bone and the capsule and synovial hypertrophy in the same area (see figures 3 and 6), while in clinical examination physicians consider tenderness, swelling and warmth of a joint. These three signs may not be directly related to the fluid built-up and hypertrophy and also depend more on subjective impression of the physicians than ultrasound images. It seems that fluid built-up inside the capsule should directly affect the optical signal. However, at this point it is not clear if the changes in the optical properties in synovial fluid in between the bones are dominating effects caused by joint effusion towards the side of the joint. Furthermore it is well known that during an inflammatory process one observes an increase blood supply (neovascularization) to the tissue surrounding the joint. This increase in blood volume may cause, for example, the warm sensation in these joints. This increase in blood volume could also explain the increased absorption coefficient in the images of affected joints and may or may not dominate effects caused by the fluid built-up visible in ultrasound images. In general, all three methods, clinical, ultrasonographic and optical tomographic examinations, appear to be sensitive to different, yet overlapping parameters which have the potential to complement each other. Further studies with a larger group of patients are necessary to fully explore these issues.

In the images shown so far we observe that the scattering and absorption images show considerable similarity. For now it remains an open question if this similarity is caused by the underlying similar spatial distribution of absorption and scattering properties in a joint, or if this similarity is an artefact brought about by the steady-state imaging method. It has been argued

that with steady-state methods, there will be cross-talk between absorption and scattering effects, and a separation between these two parameters is not possible (Arridge and Lionheart 1998). The image reconstruction problem is said to be 'ill posed.' However, some groups have suggested that with sufficient number of sources and detectors and appropriate regularization technique a separation may still be possible (Pei *et al* 2001, Iftimia and Jiang 2000, Xu *et al* 2002a).

Finally, it appears that some of the optical tomographic images display some artefacts in the close vicinity of sources and detectors (e.g., figures 4 and 5, bottom row and to lesser extent figure 5's middle row and figure 7's second column). The variations in optical properties in-between sources and detectors on the surface of the finger are most likely caused by slight differences between assumed and actual positions of sources and detectors, as well as differences between modelled and actual boundary between finger and surrounding medium. By using, for example, matching fluids or photogrammetric methods (Bluestone *et al* 2001) to more accurately determine the finger surface, one may alleviate this problem in future studies.

5. Summary

In this work we report on the first application of optical tomographic imaging methods to the assessment of finger joint inflammation (synovitis) during rheumatoid arthritis. Light from a laser diode is focused sequentially onto several points on the dorsal side of a finger immersed in water, and transillumination data are recorded along a sagittal plane on the palmar side. The recorded data are input into a model-based iterative image reconstruction scheme, which used the equation of radiative transfer as a forward model. After a detailed description of the instrumentation as well as image reconstruction procedure, we discussed two cases of patients with RA who have both been examined twice in a span of three months. The optical tomographic images are compared to clinical evaluations performed by a physician and ultrasound images. We find that optical tomographic images of joints without clinical and ultrasonographic signs of inflammation show a strong decrease of scattering as well as absorption coefficient in the general area of the joint cavity, compared to adjacent areas occupied by bone. Inflamed joints that show effusion in ultrasound images and show tenderness, swelling and warmth in clinical examination do not show this strong variation in optical properties. In these joints, the optical properties show little spatial variation or increased scattering and absorption coefficients in and around the joint cavity. To the best of our knowledge, this is the first report on an optical imaging method that allows the determination of the state of a joint, without reference to a baseline measurement. Previous studies were only able to determine the difference between two examinations on the same patients. Further studies that involve a larger number of patients are necessary to conclusively prove the clinical utility of this novel imaging modality.

Acknowledgments

This work was supported in part by a grant (R01 AR46255) from the National Institute of Arthritis and Musculoskeletal and Skin Diseases (NIAMS), which is part of the National Institutes of Health, and grants from the 'Rheumatology Competence Network' and the 'Georg-August-University Special Opportunity Research Funding' that provided funds for Dr Scheel's contributions.

References

Arnett F C *et al* 1998 The American Rheumatism Association 1987 revised criteria for the classification of rheumatoid arthritis *Arthritis Rheum.* **31** 315–24

Arridge S R and Lionheart W R B 1998 Nonuniqueness in diffusion-based optical tomography *Opt. Lett.* **23** 882–4

Backhaus M, Burmester G R, Sandrock D, Loreck D, Hess D, Scholz A, Blind S, Hamm B and Bollow M 2002 Prospective two year follow up study comparing novel and conventional imaging procedures in patients with arthritic finger joints *Ann. Rheum. Dis.* **61** 895–904

Backhaus M, Kamradt T, Sandrock D, Loreck D, Fritz J, Raber H, Hamm B, Burmester G R and Bollow M 1999 Arthritis of the finger joints—a comprehensive approach comparing conventional radiography, scintigraphy, ultrasound, and contrast-enhanced magnetic resonance imaging *Arthritis Rheum.* **42** 1232–45

Benaron D A *et al* 2000 Noninvasive functional imaging of human brain using light *J. Cereb. Blood Flow Metab.* **20** 469–77

Beuthan J, Cappius H J, Hielscher A, Hopf M, Klose A and Netz U 2001 Initial investigations of the application of linear signal transfer theory to tissue optics *Biomed. Tech.* **46** 298–303

Beuthan J, Netz U, Minet O, Klose A D, Hielscher A H, Scheel A, Henniger J and Muller G 2002 Light scattering study of rheumatoid arthritis *Quantum Electron.* **32** 945–52

Bluestone A Y, Abdoulaev G, Schmitz C, Barbour R L and Hielscher A H 2001 Three-dimensional optical-tomography of hemodynamics in the human head *Opt. Express* **9** 272–86

Boutry N, Larde A, Lapegue F, Solau-Gervais E, Flipo R M and Cotten A 2003 Magnetic resonance imaging appearance of the hands and feet in patients with early rheumatoid arthritis *J. Rheumatol.* **30** 671–9

Brown J H and Deluca S A 1995 The radiology of rheumatoid arthritis *Am. Fam. Physician* **52** 1372–80

Chance B, Alfano R R and Tromberg B J (ed) 1999 *Optical Tomography, Photon Migration and Spectroscopy of Tissue III SPIE Proc.* **3597**

Chance B, Alfano R R, Tomberg B J, Tamura M and Sevick-Muraca E M (ed) 2001 *Optical Tomography, Photon Migration and Spectroscopy of Tissue IV SPIE Proc.* **4250**

Culver J P, Choe R, Holboke M J, Zubkov L, Durduran T, Slemp A, Ntziachristos V, Chance B and Yodh A G 2003 Three-dimensional diffuse optical tomography in the parallel plane transmission geometry: evaluation of a hybrid frequency domain/continuous wave clinical system for breast imaging *Med. Phys.* **30** 235–47

Fiocco U *et al* 1996 Long term sonographic follow-up of rheumatoid and psoriatic proliferative knee joint synovitis *Brit. J. Rheumatol.* **35** 155–63

Franceschini M A, Fantini S, Thomspon J H, Culver J P and Boas D A 2003 Hemodynamic evoked response of the sensorimotor cortex measured noninvasively with near-infrared optical imaging *Psychophysiology* **40** 548–60

Fuchs H A, Brooks R H, Callahan L F and Pincus T 1989 A simplified 28-joint quantitative articular index in rheumatoid arthritis *Arthritis Rheum.* **32** 531–7

Graham T B, Blebea J S, Gylys-Morin V and Passo M H 1997 Magnetic resonance imaging in juvenile rheumtoid arthritis *Semin. Arthritis Rheum.* **27** 161–8

Gratton G, Fabiani M, Elbert T and Rockstroh B 2003 Seeing right through you: applications of optical imaging to the study of the human brain *Psychophysiology* **40** 487–91

Grosenick D, Moesta K T, Wabnitz H, Mucke J, Stroszczynski C, Macdonald R, Schlag P M and Rinneberg H 2003 Time-domain optical mammography: initial clinical results on detection and characterization of breast tumors *Appl. Opt.* **42** 3170–86

Harris E D 1990 Rheumatoid arthritis: pathophysiology and implications for therapy *N. Engl. J. Med.* **322** 1277–89

Hebden J C 2003 Advances in optical imaging of the newborn infant brain *Psychophysiology* **40** 501–10

Henniger J, Minet O, Dang H T and Beuthan J 2003 Monte Carlo simulations in complex geometries: modeling laser light transport in real anatomy of rheumatoid arthritis *Laser Phys.* **13** 796–803

Hielscher A H, Klose A D and Hanson K M 1999 Gradient-based iterative image reconstruction scheme for time-resolved optical tomography *IEEE Trans. Med. Imaging* **18** 262–71

Iftimia N and Jiang H B 2000 Quantitative optical image reconstruction of turbid media by use of direct-current measurements *Appl. Opt.* **39** 5256–61

Klose A D and Hielscher A H 1999 Iterative reconstruction scheme for optical tomography based on the equation of radiative transfer *Med. Phys.* **26** 1698–707

Klose A D and Hielscher A H 2002 Optical tomography using the time-independent equation of radiative transfer 2: Inverse model *J. Quant. Spectrosc. Radiat. Transfer* **72** 715–32

Klose A D and Hielscher A H 2003 Quasi-Newton methods in optical tomographic imaging *Inverse Probl.* **19** 387–409

Klose A D, Hielscher A H, Hanson K M and Beuthan J 1998 Two- and three-dimensional optical tomography of a finger joint model for diagnostic of rheumatoid arthritis *Proc. SPIE* **3566** 151–60

Klose A, Prapavat V, Minet O, Beuthan J and Mueller G 1997 Investigation of RA diagnostics applying optical tomography in frequency-domain *Proc. SPIE* **3196** 194–204

Klose A D, Netz U, Beuthan J and Hielscher A H 2002 Optical tomography using the time-independent equation of radiative transfer. 1: forward model *J. Quant. Spectrosc. Radiat. Transfer* **72** 691–713

Li A *et al* 2003a Tomographic optical breast imaging guided by three-dimensional mammography *Appl. Opt.* **42** 5181–90

Li D, Meaney P M, Tosteson T D, Jiang S, Kerner T E, McBride T O, Pogue B W, Hartov A and Paulsen K D 2003b Comparisons of three alternative breast modalities in a common phantom imaging experiment *Med. Phys.* **30** 2194–205

Lubeck D P 1995 The economic impact of arthritis *Arthritis Care Res.* **8** 304–10

Lund P J, Heikal A, Maricic M J, Krupinski E A and Williams C S 1995 Ultrasonographic imaging of the hand and wrist in rheumatoid arthritis *Skeletal Radiol.* **24** 591–6

NCHS 1984 National Center for Health Statistics: Disability days, United States, 1983 *Vital Health Stat.* **10** 158

Norris J (ed) 1998 *Professional Guide to Diseases* 5th Edn (Springhouse, PA: Springhouse) pp 355–60

Obrig H and Villringer A 2003 Beyond the visible—imaging the human brain with light *J. Cereb. Blood Flow Metab.* **23** 1–18

Ostergaard M *et al* 2001 Interreader agreement in the assessment of magnetic resonance images of rheumatoid arthritis wrist and finger joints—an international multicenter study *J. Rheumatol.* **28** 1143–50

Ostergaard M, Stoltenberg M, Lovgreen-Nielsen P, Volck B, Jensen C H and Lorenzen I B 1997 Magnetic resonance imaging determined synovial membrane and joint effusion volumes in rheumatoid arthritis and osteoarthritis *Arthritis Rheum.* **40** 1856–67

Ostergaard M and Szkudlarek M 2003 Imaging in rheumatoid arthritis—why MRI and ultrasonography can no longer be ignored *Scand J. Rheumatol.* **32** 63–73

Pei Y L, Graber H L and Barbour R L 2001 Normalized-constraint algorithm for minimizing inter-parameter crosstalk in DC optical tomography *Opt. Express* **9** 97–109

Pera V E, Heffer E L, Siebold H, Schutz O, Heywang-Kobrunner S, Gotz L, Heinig A and Fantini S 2003 Spatial second-derivative image processing: an application to optical mammography to enhance the detection of breast tumors *J. Biomed. Opt.* **8** 517–24

Pifferi A, Taroni P, Torricelli A, Messina F, Cubeddu R and Danesini G 2003 Four-wavelength time-resolved optical mammography in the 680–980 nm range *Opt. Lett.* **28** 1138–40

Prapavat V, Runge W, Mans J, Krause A, Beuthan J and Muller G 1997 The development of a finger joint phantom for the optical simulation of early inflammatory rheumatic changes *Biomed. Tech.* **42** 319–26

Prevoo M L, Vanthof M A, Kupper H H, Vanleeuwen M A, Vandeputte L B A and Vanriel P L C M 1995 Modified disease activity scores that include 28 joint counts—development and validation in a prospective longitudinal study of patients with rheumatoid arthritis *Arthritis Rheum.* **38** 44–8

Scheel A K, Krause A, Mesecke-von Rheinbaben I, Metzger G, Rost H, Tresp V, Mayer P, Reuss-Borst M and Müller G A 2002 Assessment of proximal finger joint inflammation in patients with rheumatoid arthritis using a novel laser-based imaging technique *Arthritis Rheum.* **46** 1177–84

Schmidt W A, Backhaus M, Sattler H and Kellner H 2003 Imaging techniques in rheumatology: sonography in rheumatoid arthritis *Z. Rheumatol.* **62** 23–33

Schwaighofer A, Tresp V, Mayer P, Krause A, Beuthan J, Rost H, Müller G A and Scheel A K 2003 Classification of rheumatoid joint inflammation based on laser imaging *IEEE Trans. Biomed. Eng.* **50** 375–82

Semble E L 1995 Rheumatoid arthritis: new approaches for its evaluation and management *Arch. Phys. Med. Rehabil.* **76** 190–201

Siegel A M, Culver J P, Mandeville J B and Boas D A 2003 Temporal comparison of functional brain imaging with diffuse optical tomography and fMRI during rat forepaw stimulation *Phys. Med. Biol.* **48** 1391–403

Steinbrocker O, Traeger C H and Batermann R C 1949 Therapeutic criteria in rheumatoid arthritis *J. Am. Med. Assoc.* **140** 659-xx

Szkudlarek M, Court-Payen M, Jacobsen S, Klarlund M, Thomsen H S and Ostergaard M 2003a Interobserver agreement in ultrasonography of the finger and toe joints in rheumatoid arthritis *Arthritis Rheum.* **48** 955–62

Szkudlarek M, Court-Payen M, Jacobsen S, Klarlund M, Thomsen H S and Ostergaard M 2003b Interobserver agreement in ultrasonography of the finger and toe joints in rheumatoid arthritis *Arthritis Rheum.* **48** 955–62

Tan A L, Wakefield R J, Conaghan P G, Emery P and McGonagle D 2003 Imaging of the musculoskeletal system: magnetic resonance imaging, ultrasonography and computed tomography *Best Pract. Res. Clin. Rheumatol.* **17** 513–28

Tromberg B J and Yodh A G (ed) 2000 *OSA Biomedical Topical Meetings 2000* OSA Technical Digests (Washington, DC: Optical Society of America)

Tromberg B J and Yodh A G (ed) 2002 *OSA Biomedical Topical Meetings 2002* OSA Technical Digests (Washington, DC: Optical Society of America)

Wang X D, Pang Y J, Ku G, Xie X Y, Stoica G and Wang L H V 2003 Noninvasive laser-induced photoacoustic tomography for structural and functional *in vivo* imaging of the brain *Nat. Biotechnol.* **21** 803–6

Winalski C S, Palmer W E, Rosenthal D I and Weissman B N 1996 Magnetic resonance imaging of rheumatoid arthritis *Radiol. Clin. North Am.* **34** 243–57

Wolfe F, Pincus T and O'Dell J 2001 Evaluation and documentation of rheumatoid arthritis disease status in the clinic: which variables best predict change in therapy *J. Rheumatol.* **28** 1712–17

Xu Y, Gu X J, Fajardo L L and Jiang H B 2003 *In vivo* breast imaging with diffuse optical tomography based on higher-order diffusion equations *Appl. Opt.* **42** 3163–9

Xu Y, Gu X J, Khan T and Jiang H B 2002a Absorption and scattering images of heterogeneous scattering media can be simultaneously reconstructed by use of dc data *Appl. Opt.* **41** 5427–37

Xu Y, Iftimia N, Jiang H B, Key L L and Bolster M B 2001 Imaging of *in vitro* and *in vivo* bones and joints with continuous-wave diffuse optical tomography *Opt. Express* **8** 447–51

Xu Y, Iftimia N, Jiang H B, Key L L and Bolster M B 2002b Three-dimensional diffuse optical tomography of bones and joints *J. Biomed. Opt.* **7** 88–92